Mn(II) Binding and Subsequent Oxidation by the Multicopper Oxidase MnxG Investigated by Electron Paramagnetic Resonance Spectroscopy

Lizhi Tao,[†] Troy A. Stich,[†] Cristina N. Butterfield,[§] Christine A. Romano,[§] Thomas G. Spiro,[∥] Bradley M. Tebo,[§] William H. Casey,[†,‡] and R. David Britt[*,†]

[†]Department of Chemistry and [‡]Department of Geology, University of California, One Shields Avenue, Davis, California 95616, United States

[§]Division of Environmental and Biomolecular Systems, Institute of Environmental Health, Oregon Health & Science University, Portland, Oregon 97239, United States

[∥]Department of Chemistry, University of Washington, Box 351700, Seattle, Washington 98195, United States

Ⓢ *Supporting Information*

ABSTRACT: The dynamics of manganese solid formation (as MnO_x) by the multicopper oxidase (MCO)-containing Mnx protein complex were examined by electron paramagnetic resonance (EPR) spectroscopy. Continuous-wave (CW) EPR spectra of samples of Mnx, prepared in atmosphere and then reacted with Mn(II) for times ranging from 7 to 600 s, indicate rapid oxidation of the substrate manganese (with two-phase pseudo-first-order kinetics modeled using rate coefficients of: $k_{1obs} = 0.205 \pm 0.001$ s^{-1} and $k_{2obs} = 0.019 \pm 0.001$ s^{-1}). This process occurs on approximately the same time scale as in vitro solid MnO_x formation when there is a large excess of Mn(II). We also found CW and pulse EPR spectroscopic evidence for at least three classes of Mn(II)-containing species in the reaction mixtures: (i) aqueous Mn(II), (ii) a specifically bound mononuclear Mn(II) ion coordinated to the Mnx complex by one nitrogenous ligand, and (iii) a weakly exchange-coupled dimeric Mn(II) species. These findings provide new insights into the molecular mechanism of manganese mineralization.
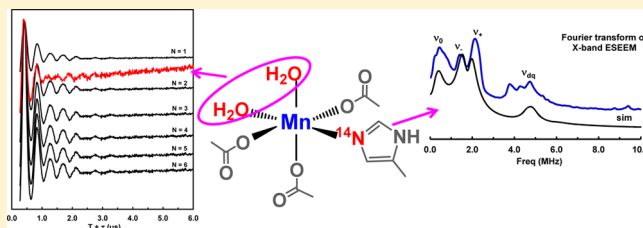
1. INTRODUCTION

A key step of the global redox cycling of manganese is the oxidation of aqueous Mn(II) to yield solid MnO_x, with the rates depending sensitively on solution pH.[1,2] In seawater (pH = 8.16), abiotic Mn(II) oxidation proceeds very slowly with a pseudo-first-order rate constant ca. 6.7×10^{-5} h^{-1}.[3] However, microorganisms (bacteria and fungi)[4−8] can speed up this process by 3−5 orders of magnitude.[2] In marine *Bacillus* bacteria, a cluster of seven genes (*mnx*A through *mnx*G) was identified as being responsible for Mn(II) oxidation.[9,10] One of these genes *mnx*G encodes a putative multicopper oxidase (MCO),[2,9−11] similar to the laccase, ascorbate oxidase, human ceruloplasmin (hCp), and Fet3p enzymes which oxidize a variety of organic and inorganic substrates coupled to reduction of O_2 to H_2O.[12,13] The MnxG protein was recently isolated as part of a multiprotein complex along with gene products MnxE and MnxF—a complex (denoted as "Mnx" in the following) with a molecular weight of ≈230 kDa.[14]

MCO enzymes contain three types of copper cofactors. Type 1 (T1), or blue copper sites, have the copper ion coordinated in a trigonal-planar-type geometry by two histidine and one cysteine side chains. An axial ligand sits above this plane and is generally a weakly bound methionine residue, but this amino acid is not strictly conserved across all T1 sites.[13] When

oxidized to the Cu(II) oxidation state, T1 sites are characterized by an intense absorption feature at ≈590 nm that is assigned to a ligand-to-metal (Cys $S_\pi \rightarrow$ Cu $3d_{x^2−y^2}$) charge-transfer transition. Oxidized T1 sites are also known to give rise to electron paramagnetic resonance (EPR) signals with a small ^{63,65}Cu hyperfine coupling ($A_\parallel \approx 4−10$ mT). These spectroscopic properties are diagnostic of the highly covalent Cu−Cys S bond. Oxidized type 2 (T2) copper (with square-planar geometry) centers exhibit larger ^{63,65}Cu hyperfine splitting value ($A_\parallel \approx 20$ mT). Oxidized type 3 (T3) copper sites are antiferromagnetically coupled binuclear Cu(II) clusters bridged by oxygen ligands (either hydroxido, oxido, or bis oxido) and tend to be EPR silent.[12,13] Some MCOs have additional copper centers: for example, hCp has two additional T1 copper sites (giving a total of six copper ions per protein).[15,16] One of these T1 sites appears to be redox active during the ferroxidase reaction, implying a mechanistic role.[16]

The MCO-catalyzed reduction of O_2 is well studied.[12,13,17−19] In the simplest case, the resting oxidized state of MCO is known to have all four copper ions in the 2+ oxidation state, and a μ_2-OH bridge exists between the two

A

copper centers of the T3 site. The T1 copper accepts electrons from substrate molecules and funnels them via intramolecular electron transfer (IET, $k_{IET} \approx 0.11$ s^{-1} at 4 °C)[17] over ≈ 13 Å to the trinuclear copper site (TNC), consisting of one T2 and a T3 site). Upon the accumulation of four electrons from substrate, the MCO is fully reduced. At this stage, exogenous O$_2$ binds to and rapidly oxidizes ($k_{eff} \approx 10^6$ M^{-1} s^{-1}) the TNC by two electrons leading to formation of the peroxy intermediate (PI). PI then rapidly decays to the so-called native intermediate (NI) that spectroscopic evidence shows to have a μ_3-oxido bridging the three copper centers of the TNC, while the μ_2-OH remains bound between the two copper centers of the T3 site.[18] In the absence of additional O$_2$, the native intermediate will slowly decay (≈ 0.007 s^{-1} at 4 °C) back to the resting, fully oxidized state.[17]

In the present paper, we examine the binding of Mn(II) substrate to the Mnx protein complex using pulse EPR spectroscopic methods. We find that one proteinaceous nitrogen ligand and two water ligands coordinate to a specifically bound mononuclear Mn(II) center. Continuous-wave (CW) EPR studies suggest that a dimeric Mn(II) species is formed early in the reaction cycle. CW EPR studies are further employed to monitor the kinetics of manganese oxidation catalyzed by the MCO and reveal that Mn(II) oxidation occurs on a time scale that is approximately equal to that for bulk MnO$_2$ formation. Collectively, these results provide new insights into the molecular mechanism of biological Mn(II) oxidation.

2. EXPERIMENTAL PROCEDURES

2.1. Sample Preparation. Protein was purified by native methods or by Strep-tag affinity[20] chromatography as described previously.[14,21] In short, MnxEFG protein was expressed from a *mnxDEFG* gene construct and loaded with Cu by incubating the static *Escherichia coli* BL21 (DE3) culture with CuSO$_4$ to allow for microaerobic *in vivo* uptake of Cu.[22] The protein was purified by a series of native chromatographic separations or on a Strep-tactin affinity column. Excess Cu was removed with extensive dialysis in 20 mM HEPES, 50 mM NaCl, pH 7.8. The protein was then concentrated and flash frozen in liquid N$_2$. Since protein yield was low (approximately 3 mg protein per L culture), samples were thawed and pooled to carry out spectroscopic studies.

In order to determine possible ligands to the T1 copper site, a comparison of the Mnx amino acid sequence against that of other MCOs was performed. His340 was identified as a potential ligand to the T1 copper.[9,10] The H340A mutant was generated by overlap extension PCR.[23] The inner primers used were 5′-GTATCCG**gc**CTTCGGC-3′ (forward) and 5′-GCCGAAG**gc**CGGA-TAC-3′ (reverse). The nucleotides in lowercase bold mark the location of a CAC → GCC mutation that encodes "A" instead of "H". The outer primers used were 5′-GTTAATACGTTCGGGGACCA-3′ and 5′-TATGCGGCATGCGATTAGTA-3′, which flank the *Hind*III and SbfI sites within the *mnxG* sequence. These restriction sites were used to clone the mutant H340A fragment into the pTXB1 overexpression plasmid, and the resulting construct was transformed into *E. coli* BL21 (DE3). The expression and purification procedure was similar to that of wild type Mnx protein complex.[14]

Reaction mixtures of Mnx with aqueous Mn(II) and O$_2$ were prepared both aerobically and anaerobically. Aerobically as-isolated oxidized Mnx was reacted with 4 equiv of MnCl$_2$ and frozen by hand after different reaction times. First, at room temperature (22 °C), 100 μL Mnx (50 μM) in a pH-buffered solution (20 mM HEPES, 20 mM NaCl, pH = 7.8, 20% ethylene glycol and saturated with O$_2$ from air) was transferred to the bottom of quartz X-band EPR tube (Wilmad PQ-706, ID = 2.8 mm, OD = 3.8 mm) using a glass pipet. Then 100 μL MnCl$_2$ (200 μM) aqueous solution saturated with O$_2$ from air was

transferred by glass pipet to mix with Mnx protein. The mixing was achieved by first bringing the tip of the pipet filled with MnCl$_2$ aqueous solution to the bottom of the EPR tube prefilled with 100 μL Mnx protein buffer solution and then by repeatedly pipetting the solution up and down in the tip for complete mixing. After being allowed to react for set times (7–600 s) at room temperature (22 °C), samples were frozen and stored in liquid N$_2$.

Fully reduced Mnx protein was prepared anaerobically in a glovebox that had been purged with N$_2$. A 5-fold excess of sodium dithionate was added to Mnx and allowed to react for 30 min during which the blue color from the T1 copper center (λ_{max} = 590 nm) bleached. Excess sodium dithionate was removed by desalting the solution using a spin column (Thermo Scientific, #89849) that had been pre-equilibrated with deoxygenated HEPES-buffered solution. A 3-fold exchange of the buffer was accomplished using 0.5 mL centrifugal filters (Amicon Ultra, #UFC510024). The resulting reduced protein was checked by X-band CW EPR spectroscopy for residual signals from Cu(II)-containing species. No such signals were observed, indicating that all the Cu(II) centers in Mnx were fully reduced by the treatment. This reduced protein solution is denoted as "RedMnx". All the Mnx-containing samples prepared for this study used either as-isolated oxidized Mnx protein complex or RedMnx.

Under anaerobic conditions, 100 μL aliquots of 50 μM RedMnx were pre-incubated with 4 equiv of MnCl$_2$ before being mixed with air-saturated ([O$_2$] $\approx$ 260 μM) HEPES buffer solution (as above). These mixtures were allowed to react for different times (23, 60, 180, and 300 s) before being hand-frozen in liquid N$_2$. The sample denoted '0 s' was obtained by mixing with deoxygenated buffer instead so that no oxidation occurred.

Samples of RedMnx that were anaerobically incubated with varying amounts of MnCl$_2$ ([Mn(II)]:[RedMnx] = 0.2, 0.8, 4.0, and 6.0 equiv) were prepared in a glovebox purged with N$_2$. To make these samples, 100 μL RedMnx was mixed with 100 μL of the appropriate MnCl$_2$ solution and allowed to incubate for 30 min in an X-band EPR tube before being frozen and stored in liquid N$_2$.

Mn(II) bound to bovine serum albumin (BSA) was prepared by mixing 100 μL 326 μM BSA (Sigma-Aldrich, CAS: 9048-46-8) in HEPES buffer solution (pH = 7.8) with 100 μL 256 μM MnCl$_2$ aqueous solution. The mixing procedure in the X-band EPR tube was identical to that of aerobically hand-quenched samples of Mnx protein and MnCl$_2$. After mixing for 5 min at room temperature (22 °C), the sample was frozen and stored in liquid N$_2$.

A sample of RedMnx was anaerobically incubated with 0.8 equiv of MnCl$_2$ in D$_2$O that had been prepared in a glovebox purged with N$_2$ in the same procedure as sample "RedMnx + 0.8Mn(II)", except that HEPES buffer in D$_2$O (20 mM HEPES, 20 mM NaCl, 20% ethylene glycol, pD = 8.2) was used for buffer-exchange procedure for three times and mixed with 0.8 ratio MnCl$_2$ in D$_2$O instead. In addition, standard samples of 237 μM MnCl$_2$ in both H$_2$O and D$_2$O as well as 220 μM MnDTPA (DTPA = diethylene triamine pentaacetic acid) in both H$_2$O and D$_2$O were prepared (with 20% ethylene glycol) as standards for water counting by electron spin–echo envelope modulation (ESEEM) spectroscopy.

2.2. Spectroscopy. X-band CW EPR spectra were recorded using a Bruker (Billerica, MA) Biospin EleXsys E500 spectrometer. Cryogenic temperatures were achieved and controlled using an ESR900 liquid helium cryostat in conjunction with a temperature controller (Oxford Instruments ITC503) and gas flow controller. For perpendicular-mode EPR ($B_0 \perp B_1$), a superhigh Q resonator (ER4122SHQE) was employed, while all parallel-mode EPR experiments ($B_0 \parallel B_1$) made use of a dual-mode resonator (ER4116DM). All CW-EPR data were collected under slow-passage, nonsaturating conditions. Spectrometer settings were as follows: conversion time = 40 ms, modulation amplitude = 0.8 mT, and modulation frequency = 100 kHz; other settings are given in corresponding figure captions.

X-band (9.47–9.53 GHz) electron-spin–echo (ESE)-detected field-swept (FS) EPR ($\pi/2$-τ-π-τ-echo) and three-pulse ESEEM spectra ($\pi/2$-τ-$\pi/2$-T-$\pi/2$-τ-echo) were collected using a Bruker EleXsys E580 spectrometer equipped with a cylindrical dielectric cavity (MD5, Bruker). Experimental parameters are given in the corresponding

figure captions. Spectral simulations were performed using the Easyspin 4.0 toolbox[24,25] within the MatLab software suite (The Mathworks Inc., Natick, MA).

2.3. Quantification of Aqueous Mn(II).

In order to determine the concentration of aqueous Mn(II) in reaction mixture EPR samples, a set of standard $MnCl_2$ samples was made with concentrations ranging from 25 to 200 μM in HEPES buffer (as described above). The X-band CW EPR is characterized by a sextet of derivative-shaped peaks split by ≈9.0 mT. These features arise from the central EPR transition ($|m_S = +1/2, m_I\rangle \leftrightarrow |m_S = -1/2, m_I\rangle$) of the high-spin ($S = 5/2$) Mn(II) split by the hyperfine interaction with the $I = 5/2$ ^{55}Mn nucleus (100% natural abundance).[26,27] The peak-to-peak amplitude of the sixth, highest-field hyperfine peak was correlated to the concentration of aqueous/high-symmetry Mn(II) after scaling to account for incident microwave power and the quality factor of the resonator. The resulting linear equation, $[Mn(II)] = 8.718 \times \text{intensity}_{\text{peak-to-peak amplitude}}$, ($R^2 = 0.995$), was used to determine the concentration of aqueous Mn(II) in reaction mixture samples (see below).

2.4. Counting Bound Waters.

The number of water ligands bound to a Mn(II) center in Mnx can be determined by evaluating the solvent-exchangeable deuterium modulation depth in three-pulse ESEEM spectra.[28] The interpulse delay value τ was set to a value equal to three times the ^{1}H precessional period at each magnetic field in order to suppress modulation from weakly coupled protons.[29] The ESEEM data of Mn(II) bound to Mnx were scaled to a value of 1.0 at the first observable maximum in the spectrum. The resultant ESEEM spectrum of the sample prepared in buffered D_2O was divided by that of an identical sample in H_2O in order to cancel out all modulations from nonexchangeable protons and from other kinds of hyperfine-coupled nuclei (i.e., ^{14}N). The resultant quotient (or "D_2O/H_2O-ratioed") spectrum consists only of modulations arising from solvent-exchangeable deuterons. These deuterons are typically found in the first- and second-coordination sphere of the Mn(II) ion (red trace, shown in Figure S1A). In order to obtain signals from only those first-coordination-sphere deuterons, the quotient spectrum was subsequently divided by the D_2O/H_2O-ratioed ESEEM spectrum of Mn(II)DTPA. Mn(II)DTPA possesses no inner-sphere exchangeable deuterons, therefore the D_2O/H_2O-ratioed spectrum (red trace, shown in Figure S1B) represents modulation arising from only second-coordination-sphere deuterons that are weakly coupled to the Mn(II) spin center. Ideally, this procedure of dividing all experimental D_2O/H_2O-ratioed ESEEM data by the D_2O/H_2O spectrum of the Mn(II)DTPA complex leaves only modulation from inner-sphere-coordinated deuterons. This procedure applied to Mn(II) in Mnx can be summarized by the equation:

$$\frac{Mn(II) + Mnx(D_2O)/Mn(II) + Mnx(H_2O)}{Mn(II)DTPA(D_2O)/Mn(II)DTPA(H_2O)}$$

It is most likely that the inner-sphere deuterons detected this way are part of ligand waters. In order to determine how many waters ligate the Mn(II) center, we compare the resultant first-coordination-sphere deuterium-modulation depth to that for aqueous Mn(II) (aq) ion made by dissolving $MnCl_2$ in either H_2O or D_2O buffers, yielding either $[Mn(OH_2)_6]^{2+}$ or $[Mn(OD_2)_6]^{2+}$ ions (shown in Figure S1C). Standard modulation patterns for the case where there are less than six water ligands can be generated from the $MnCl_2$ data by taking the 1/6, 2/6, 3/6, 4/6, and 5/6 root of the inner-sphere deuterium modulation for the D_2O/H_2O-ratioed of aqueous Mn(II) (Figure S1D). As an added check for contributions from paramagnetic contaminants (e.g., Cu(II) from Mnx), this procedure was performed at two magnetic field positions, 327.3 and 363.0 mT, the latter being one at which Cu(II) resonances do not contribute.

3. RESULTS

3.1. EPR Characterization of Copper in Mnx Protein Complex.

The large molecular weight ≈230 kDa of the Mnx complex was validated by gel filtration. Based on the predicted amino acid sequence of the *mnx* gene products, this molecular weight can be obtained from oligomerization of a combination of between 6 and 8 copies of MnxE and F with one MnxG.[14,21] The Mnx protein has been analyzed for metal content previously using inductively coupled plasma-optical emission spectroscopy, and these analyses reveal ≈10 copper ions per protein complex.[14] Amino acid sequence analysis and other biochemical assays suggest that there is only one T1 copper site and one dinuclear T3 copper site in the complex, leaving approximately seven copper centers of the T2 variety.[9,10]

The as-isolated, oxidized Mnx protein was analyzed by X-band (9.68 GHz) CW EPR spectroscopy, and the corresponding spectrum (blue trace, top of Figure 1) is dominated by contributions from at least two classes of T2 copper sites as well as the T1 site. The oxidized T3 site is expected to be EPR-silent (*vide supra*). EPR spectra of T2 coppers are axial with $g_\parallel > g_\perp$ and possess a quartet of ^{63,65}Cu hyperfine lines (both copper
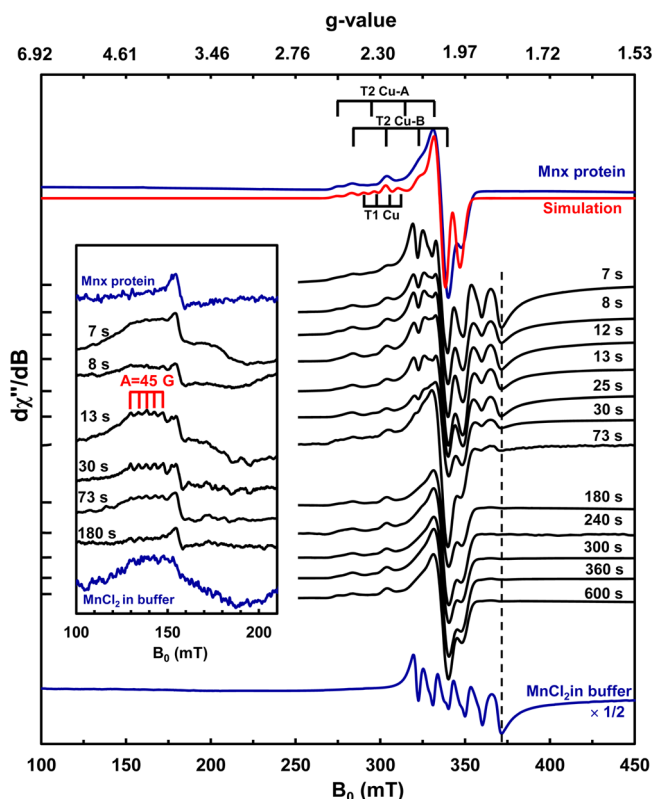

Figure 1. X-band CW EPR spectra of Mnx protein samples mixed with Mn(II) and hand-quenched in air after being allowed to react for times ranging from 7 to 600 s. The ratio of $MnCl_2$ to Mnx protein was 4 at time = 0 s; 100 μL of 50 μM Mnx protein mixed with 100 μL of 200 μM $MnCl_2$ (total volume: 200 μL); both solutions were saturated with O_2 from air. Spectra of as-isolated Mnx protein (topmost blue trace) and 100 μM $MnCl_2$ in buffer (bottommost blue trace) are presented for comparison. Inset shows the low field spectral region around $g = 4.3$ ($B_0 = 155$ mT). Experimental parameters: temperature = 15 K; microwave frequency = 9.68 GHz; microwave power = 0.6325 mW; conversion time = 40 ms; modulation amplitude = 0.8 mT; modulation frequency = 100 kHz. Simulation (red trace) of the as-isolated Mnx complex was achieved using three spectroscopically distinct Cu(II) species: $g_1 = [2.065\ 2.050\ 2.305]$ and $A_1 = [45\ 45\ 210]$ MHz for T1 Cu; $g_2 = [2.035\ 2.055\ 2.280]$ and $A_2 = [27\ 27\ 600]$ MHz for T2 Cu−A; $g_3 = [2.055\ 2.050\ 2.210]$ and $A_3 = [30\ 30\ 600]$ MHz for T2 Cu−B; with arbitrary ratio of 1:1:2 for T1 Cu:T2 Cu−A: T2 Cu−B.

isotopes, ^{63}Cu, 69% abundant, and ^{65}Cu, 31% abundant, are I = 3/2) centered at the field position corresponding to $g_{\parallel}$ with splittings of approximately 20 mT (560 MHz). One class of T2 signals is characterized by $g_{\parallel}$ = 2.28 $A_{\parallel}$ = 600 MHz (denoted as T2 Cu−A) and the other has $g_{\parallel}$ = 2.21 $A_{\parallel}$ = 600 MHz (denoted as T2 Cu−B); results consistent with those observed previously.[21]

As up to seven T2 copper sites contribute to the EPR spectrum, it is difficult to unambiguously assign the signal arising from the lone T1 copper center. Sequence analysis identified a possible histidine ligand (His340) to the T1 site of the MnxG protein.[9,10] In mutating this residue to alanine (H340A), the blue color of the Mnx protein was lost (Figure S2A), signaling that the electronic structure of T1 copper site was significantly perturbed. The EPR spectrum of this H340A mutant (green trace shown in Figure S2B) shows loss of two narrower signals at 275.0 to 286.0 mT in the spectrum of the oxidized wild-type (WT) Mnx, which we assign to T1 Cu with $g_{\parallel}$ = 2.30 $A_{\parallel}$ = 210 MHz. This H340A mutant can still bind copper at the T1 binding site, however, the modified ligand set leads to a change of the copper ion electronic structure properties. Canters and co-workers[30] reported that an analogous His-to-Ala mutation to the T1 site ligand set in nitrite reductase altered the redox properties of this site such that it could only be oxidized in the presence of exogenous ligands (either imidazole or chloride). Therefore, one reason for the loss of the T1 Cu EPR signal from the spectrum of the H340A mutant of Mnx could be due to it being locked into the reduced form.[31]

Some of the T2 copper centers are also likely found in the MnxE and MnxF proteins; whether these are involved in manganese oxidation is unknown. While future spectroscopic investigations will explore more precisely the distribution of coppers about the Mnx protein complex, for the present study, we have established that both T1 and T2 copper sites are spectroscopically observable, consistent with all other MCOs. This EPR spectrum of Mnx in its as-isolated, oxidized state will serve as the starting point for our analysis of spectral changes incurred during Mnx-catalyzed Mn(II) oxidation described next.

3.2. Kinetics of Mn(II) Oxidation. As-isolated, oxidized Mnx protein was mixed in air with a solution containing 4 equiv of Mn(II) in atmosphere-equilibrated buffer ([solvated O_2] ≈ 260 μM). The aging time of the reaction mixtures was varied from 7 to 600 s after which the reaction was quenched by freezing the samples in liquid nitrogen. X-band (9.68 GHz) CW EPR spectra were then collected (Figure 1, black traces). In the spectra of the early freeze-quenched samples (frozen within 73 s of mixing), we observe the iconic sextet of derivative-shaped peaks for Mn(II)-containing species (cf. bottommost trace corresponding to aqueous MnCl$_2$ in Figure 1) in addition to signals for the T1 and T2 copper sites described in Section 3.1 above (top trace in Figure 1). This aqueous Mn(II) EPR signal will be denoted as the "class i" signal for the remainder of this work. As described in the Experimental Procedures section, we used the peak-to-peak intensity of the sixth, highest-field EPR feature of this Mn(II) sextet (peak at 369.0 mT, vertical dotted line in Figure 1) as an indicator of aqueous Mn(II) concentration during turnover. This signal rapidly decreases in intensity with increasing aging time (Figure 2, red circles). Samples frozen after 73 s of reaction are completely devoid of aqueous Mn(II) signals.
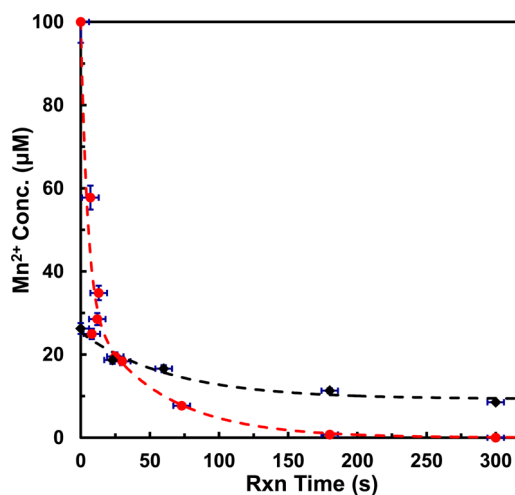

Figure 2. Aqueous Mn(II) concentration measured by CW EPR in freeze-quenched mixtures of Mnx and MnCl$_2$ as a function of reaction time. Red-filled circles correspond to data in Figure 1 from samples prepared aerobically. Black diamonds correspond to data in Figure 3 from samples prepared anaerobically before being mixed with an O$_2$-containing buffer solution. Dashed lines correspond to fits obtained using pseudo-first-order kinetics. For the aerobic data set, two phases were employed with k_{1obs} = 0.205 s^{-1} and k_{2obs} = 0.019 s^{-1}. For the anaerobic data set, one phase was employed with k_{obs} = 0.015 s^{-1}. Free Mn(II) concentrations were determined using the relation [Mn(II)] = 8.71 × intensity$_{peak-to-peak\ amplitude}$, ($R^2$ = 0.995) as described in the Experimental Procedures section.

This signal loss is attributed to either oxidation of the substrate to the 3+ or 4+ oxidation state or coordination of the formerly aqueous Mn(II) ion in a binding site that induces a significantly larger zero-field splitting (ZFS) interaction, which would broaden the monitored EPR feature possibly beyond detection.[26,27,32,33] Given these two possibilities, the data (red circles) in Figure 2 were fit using a biphasic kinetic model (red circles) dashed line in Figure 2. The major component (≈68.7%) had an effective rate constant of k_{1obs} = 0.205 ± 0.001 s^{-1} and the minor component (≈31.3%) had k_{2obs} = 0.019 ± 0.001 s^{-1}.

We tentatively assign the more rapid process to the binding of Mn(II) to a specific site within the Mnx complex, although the exact K_d is unknown. The slower process is assigned to substrate oxidation as the observed rate of Mn(II) oxidation is quite similar to the reported rate Fe(II) oxidation by *Rhus vernicifera* laccase (0.029 s^{-1} at 25 °C, pH = 7.0).[34] We note, however, that faster single turnover kinetics are reported for Fe(II) oxidation catalyzed by other MCO metallo-oxidases, e.g., the reduction rate constant for the T1 Cu in Fet 3p is >1200 s^{-1} (4 °C, pH = 7.0)[35] and in hCp it is >150 s^{-1} (25 °C, pH = 7.0).[16,34] Both of these processes are on the same time scale as the rate of formation of bulk solid MnO$_x$ measured by electronic absorption spectroscopy (λ_{max} ≈ 380 nm).[14]

Though the Mn(II) signal decreases monotonically with time, the signals for T2 copper sites are evident at all times (Figure 1). During the reaction, subtle changes in relative intensities of the various Cu(II) signals do occur, though a complete analysis of these changes is beyond the scope of this study.

In addition to the loss of the aqueous Mn(II) signal, there is a new multiplet apparent at lower field that appears in the spectra of early reaction mixtures and eventually decays away (see inset of Figure 1). In the spectrum of the sample freeze-

quenched at 13 s, one can clearly see a regular splitting of approximately 4.5 mT between at least five lines ca. 136.0 mT (we call this the "class iii" signal, *vide infra*). This field position, corresponding to $g \approx 5.0$, is typically where the most intense features of high-spin, $S = 3/2$, Mn(IV)-containing species are found.[36−40] However, we disfavor this assignment as similar features are also present in the spectrum of a sample of anaerobically prepared, dithionite-reduced Mnx that had been incubated with Mn(II) (see top trace in inset of Figure 3).
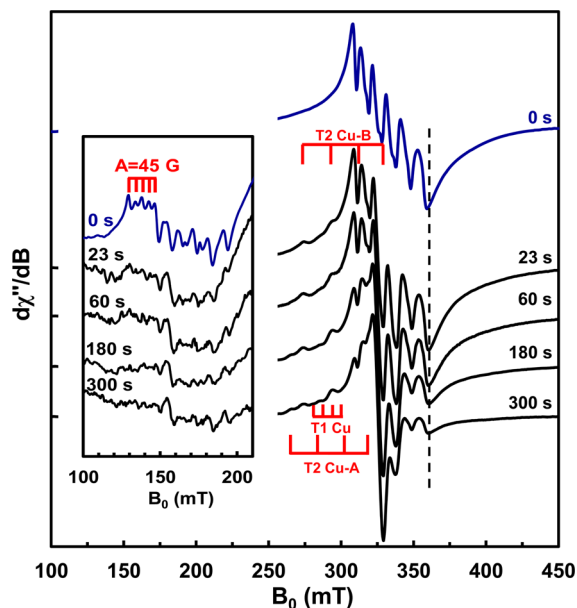

Figure 3. X-band CW EPR spectra of anaerobically prepared samples of RedMnx protein pre-incubated with 4 equiv Mn(II) and hand-quenched after being allowed to react with an O_2-containing solution for times ranging from 0 to 300 s. 100 μL of 50 μM RedMnx protein and 200 μM Mn(II) was mixed with 100 μL buffered solution saturated with O_2 from air (total volume: 200 μL). Topmost, blue trace is the spectrum of a sample that was not reacted with O_2. Inset shows the low field spectral region around $g = 4.3$ ($B_0 = 155$ mT). Experimental parameters: temperature = 15 K; microwave frequency = 9.37 GHz; microwave power = 0.6325 mW; conversion time = 40 ms; modulation amplitude = 0.8 mT; modulation frequency = 100 kHz.

Absent from the spectrum of this anaerobic preparation are any signals from T1 or T2 sites in the Cu(II) oxidation state. With no oxidized copper centers and no O_2, there is no way for Mnx to oxidize Mn(II) to Mn(IV).

Instead, we suggest that the multiplet at 136.0 mT arises from two spatially close, weakly exchange-coupled Mn(II) ions. The typical EPR features for such a spin system contain 11 lines (with a 1:2:3:4:5:6:5:4:3:2:1 intensity pattern) split by ≈4.5 mT due to equivalent hyperfine interactions with both [55]Mn nuclei.[33,41] Isolated Mn(II) ions generally possess an isotropic [55]Mn hyperfine coupling constant between 8.5 and 9.0 mT, so the observed coupling of 4.5 mT in this case is strongly indicative of a dimeric Mn(II,II) species.[42] That we observe just five peaks with roughly equal intensity could be due to our only seeing the central five features of the undecaplet with 4:5:6:4:5 intensity, and the other features are simply not resolved.[43,44] Similar [55]Mn hyperfine patterns are also observed from Mn(II,II) species in manganese-bound DNA-binding protein from nutrient starved cells.[45] For the reactions of Mn(II) with as-isolated, oxidized Mnx that were performed in the presence

of O_2, this multiplet is only observed in spectra of samples frozen after an aging times of 13 s but disappears from those aged longer than 180 s. This behavior suggests that the putative dimer takes some time to form from aqueous Mn(II) ions before it becomes spectroscopically silent again—presumably as a result of manganese-centered oxidation—consistent with the biphasic kinetics of Mn(II) signal loss that we observe (Figure 2).

To test this hypothesis, we investigated the oxidation of Mn(II) by RedMnx protein that was pre-incubated with 4 equiv Mn(II) and then reacted with O_2-saturated buffer solution, yet maintained in a N_2 atmosphere. As mentioned previously, by pre-incubating Mnx with Mn(II), we assume that the substrate-binding site is already loaded with Mn(II) before the reaction begins. The aging times after mixing were varied from 0 to 300 s. The corresponding EPR spectra of these reaction mixtures are shown in Figure 3. For the first time point (no O_2 added), a typical Mn(II) sextet centered at $g \approx 2.0$ is observed as well as the multiplet tentatively assigned to a Mn(II,II) species centered at 136.0 mT. In addition to this signal at 136.0 mT from the Mn(II,II) dimer, there is a sextet of EPR features centered at 170 mT and split by 9.0 mT (top spectrum, Figure 3 inset) that we assign to the half-field transition of a Mn(II)-containing species with a modest ZFS value ($D \approx 1000$ MHz).[26,27] Indeed, an acceptable preliminary simulation of the signal is achieved using $D = 1080$ MHz and $E = 356$ MHz (Figure S3). Higher-field EPR spectroscopic studies are underway to determine the ZFS parameters more assuredly. We will refer to this manganese center as the "class ii" mononuclear Mn(II) species for the remainder of this work. ZFS arises from the introduction of angular momentum in the ground electronic state caused by molecular distortions and leads to the breaking of the degeneracy of the $M_s = |\pm1/2\rangle$, $|\pm3/2\rangle$, $|\pm5/2\rangle$ Kramers doublets of the $S = 5/2$ Mn(II) ion in the absence of an applied magnetic field. The energy spacing between these levels goes as DM_s^2 (where D is the axial ZFS parameter) and further by a function of E (the rhombic term). This rhombic distortion for Mn(II) centers leads to mixing spin states differ by $M_s = \pm 2$, providing possibilities for transitions between levels that formally differ by $\Delta m_s = \pm 2$.[26,27] This will give rise to EPR features at half the resonant field position for a free electron.[46−52] We see some evidence of these half-field features in the data presented in Figure 1 (see traces corresponding to 13 and 30 s freezing times), but clearly the concentration of the corresponding Mn(II)-containing species is quite low.

Once the samples are reacted with O_2, Cu(II) EPR signals appear, and all three Mn(II) signals start to diminish in intensity monotonically. Again, by monitoring the sixth [55]Mn hyperfine peak at 360 mT (vertical dotted line in Figure 3), we have determined aqueous Mn(II) concentration as a function of mixing time (presented in Figure 2, black diamonds). This signal loss is well-modeled (black dashed line) by a single decaying exponential with $k_{obs} = 0.015 \pm 0.001$ s^{-1}. That not all of the Mn(II) signal is gone at long reaction times suggests that the dissolved O_2 in the starting mixture is exhausted before complete Mn(II) oxidation. This k_{obs} is comparable to that found for the slower process causing loss of the Mn(II) EPR signal in the presence of atmospheric O_2 ($k_{2obs} = 0.019 \pm 0.001$ s^{-1}).

We also looked for EPR spectroscopic signatures of higher oxidation states of manganese in either mononuclear or multinuclear species. At no point did we observe parallel-

mode EPR signals that would possibly correspond to a mononuclear S = 2 Mn(III) species (data not shown).[52−54] However, the zero-field splitting parameters of a Mn(III) spin system could be too large or too heterogeneous to see the corresponding signals. Also, Mn(III) is a potent oxidant and disproportionates rapidly unless strongly ligated to a compound such as pyrophosphate.[55−57] We also saw no evidence of multiline signals that would result from two antiferromagnetically coupled Mn ions giving rise to a net S = 1/2 electron spin, e.g., a Mn(II,III)[58] or a Mn(III,IV) species.[44,59] As for possible mononuclear Mn(IV) complexes, again we observe no obvious signals in the $g \approx 4.0$ region that would be diagnostic of such S = 3/2 species (see above discussion). However, we know that a Mn(IV)-containing species is ultimately produced and incorporated into the product, solid manganese oxide MnO$_x$, although it is not clear how long this species exists as a monomer (if at all) since the Mn(IV) oligomerizes extensively at all but very low pH conditions.[60] Experiments in our laboratories will continue to target these putative higher-oxidation-state intermediates that lead to MnO$_x$(s) generation from Mn(II).

3.3. EPR Characterization of Mn(II) Bound To Mnx.

Fully reduced Mnx protein that was anaerobically incubated with 0.8 equiv of Mn(II) yields the CW EPR spectrum ("RedMnx + 0.8 Mn(II)") shown in Figure 4 (green traces).
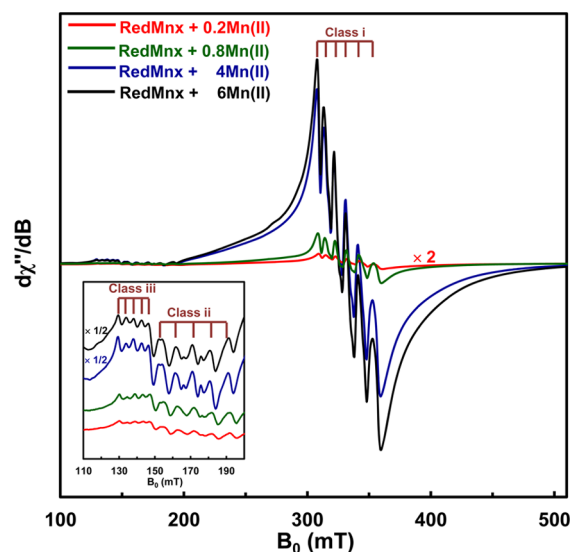

Figure 4. X-band CW EPR spectra (normalized to total [Mn]) of RedMnx protein incubated anaerobically with varying ratios (0.2, 0.8, 4, and 6) of MnCl$_2$. Inset shows the low field spectral region around g = 4.3 (B_0 = 155 mT). Experimental parameters: temperature = 15 K; microwave frequency = 9.37 GHz; microwave power = 0.6325 mW; conversion time = 40 ms; modulation amplitude = 0.8 mT; modulation frequency = 100 kHz.

Again, no Cu(II) signals are evident, confirming that the Mnx complex is completely reduced. Even at this relatively low manganese loading, all three classes of Mn(II) signals described above are seen in the spectrum: namely, those that are diagnostic of a (i) mononuclear, likely aqueous, Mn(II) species experiencing a weak ZFS interaction; (ii) a mononuclear Mn(II) species with a modest ZFS interaction; and (iii) a weakly exchange-coupled Mn(II,II) dimeric species. There is also a small amount of contaminating Fe(III) species giving rise to the signal at $g \approx 4.3$.[61]

The samples with substoichiometric manganese—0.2 equiv (red trace, Figure 4) and 0.8 (green trace, Figure 4) equiv— give rise to EPR signals centered at approximately 160 mT ascribed to class ii and class iii Mn(II) species. The spectra of samples made with 4 equiv of substrate or more (blue and black traces, Figure 4) possess two additional narrow peaks (ca. 165.0 and 174.0 mT). They could be part of an undecaplet arising from another two weakly exchange-coupled Mn(II) ions whose binding sites are populated only at these higher Mn:Mnx ratios (4:1 and 6:1). This could, to some extent, confirm our hypothesis that multiple Mn(II) binding sites exist from nearby to the T1 copper site to the surface of Mnx complex. Three sets of undecaplets with varying effective g values arising from different Mn(II)−Mn(II) species in manganese-bound DNA-binding protein from nutrient starved cells are reported by Hayden et al.[45] Alternatively, the peaks at 165.0 and 174.0 mT could arise from just a different EPR transition of the class iii dimer[41,44,62−65] and happen to be evident only at high concentrations of Mn(II) relative to the Mnx complex. Preliminary EPR spectral simulations are provided in Figure S4 to illustrate the sensitivity of the spectra of these spin systems to modest changes in various spin Hamiltonian parameters.

The temperature dependence of the EPR spectral features for the class ii and iii Mn(II)-containing species is presented in Figure 5. The intensity of the half-field transitions assigned to the class ii Mn(II) center (red filled diamonds, Figure 5B) increases with increasing temperature (over the temperature range explored, 4.5−60 K) until approximately 20 K at which time it then behave according to Curie law, indicating that this feature arises from EPR transitions between spin levels of an energetically excited spin manifold.[66] This behavior is consistent with an S = 5/2 spin center experiencing a modest positively signed ZFS interaction (D > 1000 MHz) suggesting pseudo-octahedrally coordinated Mn(II) ion.[32] For the signals assigned to the binuclear Mn(II,II) site (blue filled circles, Figure 5B), as the temperature is increased to 40 K, the intensity of the class iii multiplet increases, indicating that the donor spin levels operative in the EPR transition become more populated.[33,41] This behavior is consistent with weak antiferromagnetic coupling between the two ions, i.e., the isotropic-exchange-coupling term J is negative in the Heisenberg−Dirac−van Vleck Hamiltonian (H = $-2J\,S_1S_2$). Increasing the temperature further leads to a decrease in the intensity of the class iii signal at 135 mT, suggesting that this multiplet could arise from low-lying spin manifold which is depopulated at higher temperatures.

We further interrogated the coordination environment of the class ii Mn(II) center using ESEEM spectroscopy. The X-band (9.47 GHz) three-pulse ESEEM spectrum of RedMnx treated with 0.8 equiv of Mn(II) is shown in Figure 6A (black trace; corresponding echo-detected EPR spectrum is shown in Figure S5). These data were collected in resonance with the lowest-field member of the central sextet (314.0 mT). The corresponding Fourier transform is given in Figure 6B and shows a set of sharp peaks at 0.4, 1.4, and 2.0 MHz as well as a 3 MHz broad feature centered at 4.4 MHz. These features are assigned, respectively, to the ν_0, ν_-, ν_+ nuclear quadrupole transitions and to ν_{dq}, a double quantum transition, of a hyperfine-coupled ^{14}N-containing (I = 1) ligand to manganese.[67,68] The peak at 13.4 MHz ($\approx$ Larmor frequency of ^{1}H at 314.0 mT) is attributed to weakly hyperfine-coupled protons. Similar spectra have been observed for several Mn(II)-
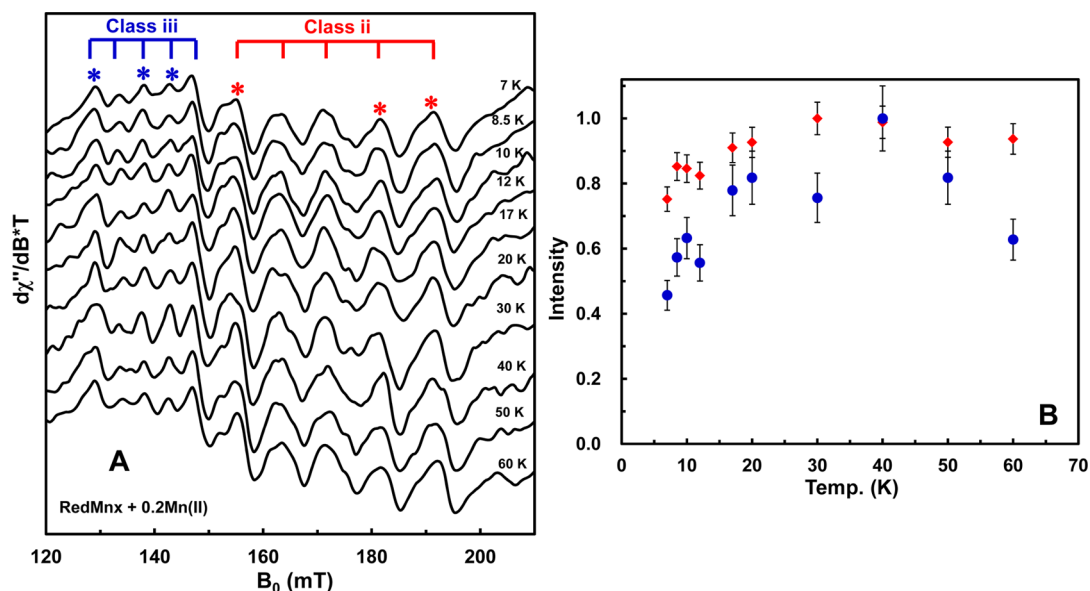
Figure 5. (A) Temperature dependence of EPR signals that appear around $g = 4.3$ ($B_0 = 155$ mT) for RedMnx mixed with 0.2 equiv Mn(II). Experimental parameters: microwave frequency = 9.37 GHz; conversion time = 100 ms; modulation amplitude = 0.8 mT; modulation frequency = 100 kHz. (B) Temperature dependence of the average peak-to-peak amplitudes of the EPR features centered at 128.3, 136.0, and 141.0 mT (blue circles) and the EPR features centered at 155.3, 181.6, and 190.0 mT (red diamonds) that correspond to the class iii and class ii Mn(II) species, respectively.
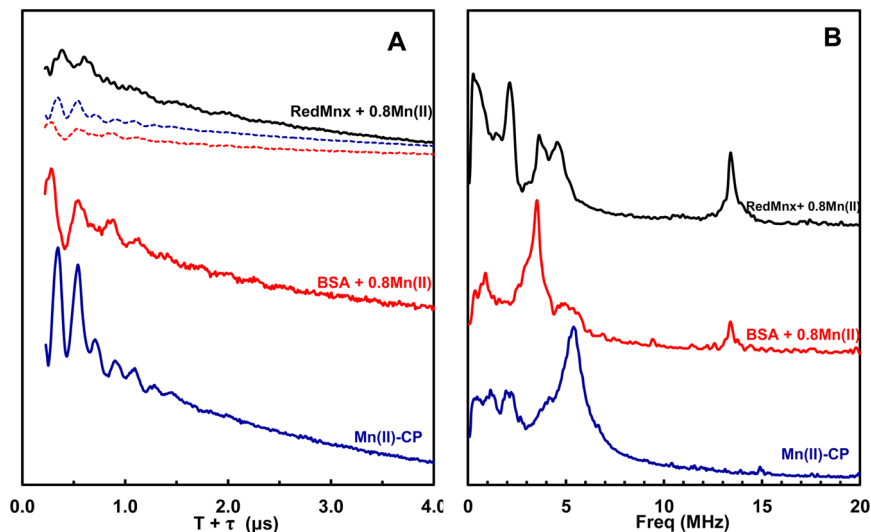

Figure 6. (A) Three-pulse ESEEM spectra of RedMnx mixed with 0.8 equiv Mn(II) (black), Mn(II) bound to BSA (red), and Mn(II) bound to CP (blue). (B) Corresponding cross-term averaged Fourier transforms of data in A. Experimental parameters (top to bottom): temperature = 10 K, microwave frequency = 9.47 GHz, $B_0 = 314.0$ mT, $\pi/2 = 16$ ns, $\tau = 140$ ns, $T = 80$ ns; temperature = 10 K, microwave frequency = 9.37 GHz, $B_0 = 314.0$ mT, $\pi/2 = 16$ ns, $\tau = 140$ ns, $T = 80$ ns; temperature = 10 K, microwave frequency = 9.55 GHz, $B_0 = 342.5$ mT, $\pi/2 = 8$ ns, $\tau = 100$ ns, $T = 136$ ns. Sixth root of Mn(II)-CP ESEEM time domain spectrum (blue dashed line) and fourth root of Mn(II)-BSA ESEEM time domain spectrum (red dashed line) are shown in A for comparison.

containing proteins,[67−69] in particular, concanavalin A (ConA), which is known to have a single histidine ligand to the metal center.[70]

In our case, we do not know the number of nitrogenous ligands and cannot determine this information from the Fourier transformed ESEEM spectrum (Figure 6B). Instead, by analyzing the depth of the ^{14}N modulations in the time-domain spectrum (Figure 6A) and comparing this depth to similar ESEEM traces for mononuclear Mn(II) bound to a known number of nitrogen ligands, we can roughly estimate the number of nitrogens bound to the class ii Mn(II) center in

Mnx. The two systems we chose for this comparison are Mn(II) bound to BSA[71] and Mn(II) bound to calprotectin (CP).[72,73] BSA contains a typical amino-terminal Cu(II)- and Ni(II)-binding motif (ATCUN) that consists of one α-amino nitrogen, two peptide nitrogens, and one imidazole nitrogen of histidine, four metal-binding nitrogen ligands in all.[71,74−76] This ATCUN motif binds Cu(II) ($\log K_f \approx 12.0$)[77,78] and Ni(II) ($\log K_f \approx 10.0$)[79] with high affinity and with somewhat lower affinity for Mn(II) ($\log K_f \approx 4.0$).[80,81] CP is a manganese sequestration protein and in the presence of 40 equiv Ca(II) binds Mn(II) tightly ($K_d = 194 \pm 203$ nM).[72] X-ray crystal
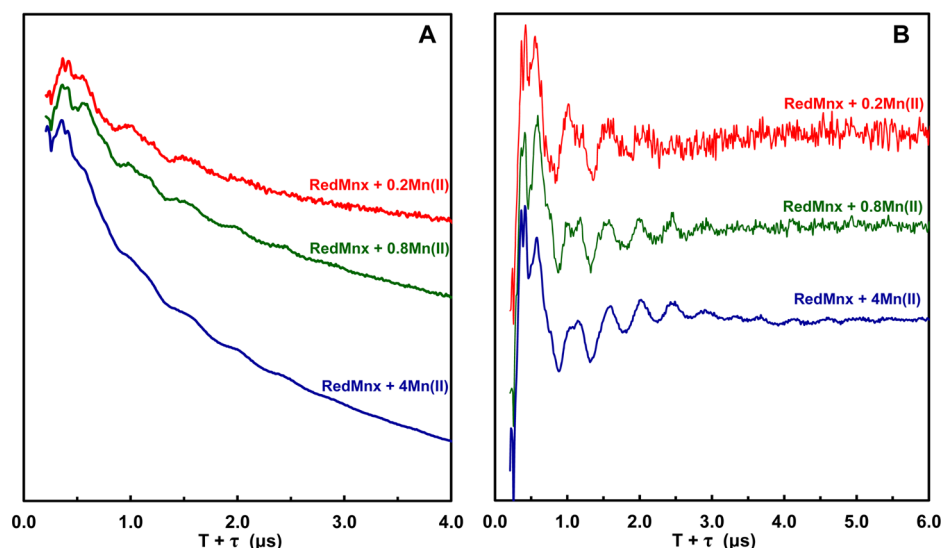
Figure 7. Three-pulse ESEEM spectra of RedMnx protein incubated with 0.2 (red traces), 0.8 (green traces), and 6 (blue traces) equiv Mn(II): (A) Raw time domain spectra; (B) same data as in A after subtracting a decaying exponential function to account for electron spin relaxation and unmodulated ESEEM from aqueous Mn(II). Experimental parameters: temperature = 10 K; microwave frequency = 9.53 GHz, B_0 = 363.0 mT, $\pi/2$ = 16 ns, τ = 128 ns, T = 80 ns.
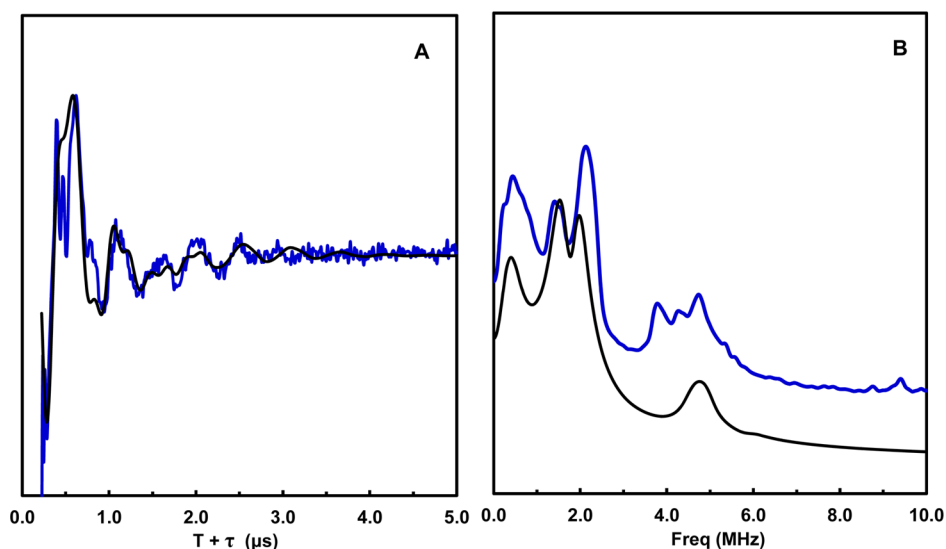

Figure 8. (A) Simulation (black traces) of three-pulse ESEEM spectrum (blue traces) of RedMnx mixed with 0.8 equiv Mn(II) and corresponding cross-term averaged Fourier transform. (B) Simulation parameters: one ^{14}N nucleus was employed with A_{iso} = +2.38 ± 0.01 MHz, A_{aniso} = [0.01 0.20−0.21] MHz, e^2Qq/h = 2.33 ± 0.01 MHz, η = 0.22 ± 0.01, and Euler angles for the NQI frame relative to the principal axes of hyperfine tensor are α = 0 ± 5°, β = 90 ± 5°, γ = 0 ± 5°. Experimental parameters: temperature = 10 K, microwave frequency = 9.53 GHz, B_0 = 327.3 mT, $\pi/2$ = 12 ns, τ = 144 ns, T = 80 ns.

structures of CP show Mn(II) is bound by six histidine side chains.[73] The ESEEM traces of substoichiometric Mn(II) bound to each of these two protein systems are shown in Figure 6A,B (time and frequency domain, respectively) and compared to those for RedMnx + 0.8 equiv Mn(II).[82,83] Qualitatively, one can see that the modulation depth evident in the ESEEM spectrum of Mn(II)-BSA (red trace) is deeper than that for Mn(II)-Mnx (black trace), and the modulation depth measured for Mn(II)-CP (blue trace) is deeper still. This trend suggests that Mnx provides less than four nitrogen ligands to the class ii Mn(II) center.

In general, the depth of ESEEM modulation is governed the number of hyperfine-coupled nuclei and the facility of nuclear spin level "branching" due to the nonsecular contribution to the

hyperfine tensor and nuclear quadrupole interactions (collectively, this branching is described by the so-called Mims matrix).[84] More specifically, for three-pulse ESEEM spectroscopy, the modulation observed in the time-domain spectrum is given by $V_{3p}(\tau,T) \propto \sum_\theta (\prod_q V_{3p}^\alpha(q,\theta) + \prod_q V_{3p}^\beta(q,\theta))$. The term $V_{3p}^{\alpha(\beta)}(q,\theta)$ describes the contribution to the modulation by nucleus q with orientation θ relative to the external static magnetic field. The modulations from all like-oriented nuclei contributing via the same coherence transfer pathway (α or β) are multiplied according to the product rule; then the products from each coherence transfer pathway are added. Finally, this result is summed over all possible orientations to give the total observed echo envelope modulation. In practice, the previous equation essentially provides a "product rule" description of the

Table 1. Measured HFI and NQI Parameters of ^{14}N Nuclei Coupled to Mn(II)

species	^{14}N	A_{iso} (MHz)	A_{aniso} (MHz)	e^2Qq/h (MHz)	η	ref
imidazole	imino	−	−	3.3	0.13	87
	amino	−	−	1.43	0.99	87
L-histidine	imino	−	−	3.36	0.13	87
	amino	−	−	1.44	0.92	87
Mn(II)-RNA	histidine	2.30	−	2.90	0.40	67
Mn(II)GMP^a	guanosine	3.00	0.65	3.20	0.30	68
	guanosine	2.10	0.40	2.90	0.40	68
Mn(II)ADP	−	2.50	−	2.60−3.10	0−1	88
Mn(II)Im$_6$	−	3.19	0.63	3.0	0.1−0.3	89
Mn(II)-Mnx	n.a.	2.38	[0.01 0.20 −0.21]	2.33 ± 0.01	0.22 ± 0.01	this work

^{a}Mn(II)GMP =: guanosine 5′-monophosphate.

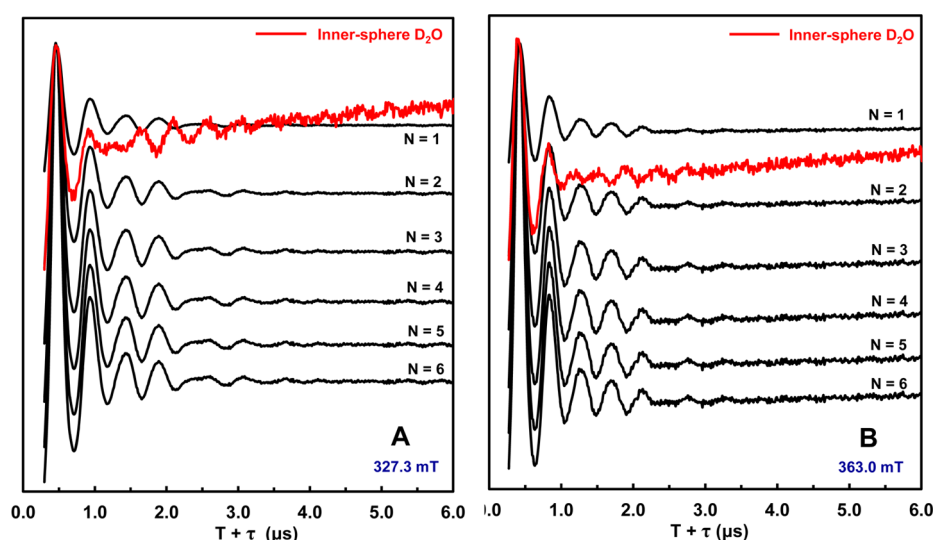**Figure 9.** D$_2$O/H$_2$O ratioed ESEEM spectrum of RedMnx mixed with 0.8 equiv Mn(II) (red traces) measured at two resonance field positions (A) 327.3 and (B) 363.0 mT. From this residual deuterium modulation, 20% of the residual deuterium modulation from $[Mn(D/H_2O)_6]^{2+}$ was subtracted to account for the small amount of class i, aqueous Mn(II) that contributes to the spectrum. This resultant trace is compared to that obtained for a various number of water ligands to the Mn(II) center (black traces) that were calculated from the D$_2$O/H$_2$O ratioed ESEEM spectra of $[Mn(D/H_2O)_6]^{2+}$ (Figure S1D) as described in the Experimental Procedures section.

observed ESEEM modulation, whereby the modulation patterns for each isolated hyperfine-coupled nucleus can be multiplied together yielding the net modulation pattern.[85] For multiple nuclei whose nuclear quadrupole and hyperfine interaction parameters are similar, e.g., the six histidine nitrogens coordinating the manganese center in CP are magnetically identical,[83] the experimental modulation pattern can be thought of as the ESEEM spectrum of one of these nitrogens raised to the sixth power.

Therefore, by taking the fourth and sixth roots of ESEEM spectra of Mn(II) bound to BSA and CP, respectively, we can visualize the modulation depth of a single ^{14}N ligand to manganese (see dashed red and blue traces, Figure 6A). We find that the arithmetically scaled spectra of Mn(II)-CP and Mn(II)-BSA give a nearly identical modulation depth to that observed for Mn(II) bound to Mnx spectrum (black solid line) indicating that just one ^{14}N-containing ligand in Mnx binds Mn(II).[86]

To confirm that this ^{14}N modulation is from a specifically bound and not an adventitiously bound Mn(II) center, we conducted ESEEM studies on samples of RedMnx containing 0.2, 0.8, and 4.0 equiv of Mn(II) (Figure 7A). As the concentration of Mn(II) relative to Mnx is increased, there is a

significant increase in the exponential decay of the three-pulse ESEEM. However, fitting and subtracting this exponential function from the data yields modulation patterns that are nearly identically deep (Figure 7B; corresponding Fourier transforms of these data can be found in Figure S6). This behavior indicates that two classes of Mn(II) species contribute to the ESEEM spectra: one is the aqueous/adventitiously bound Mn(II) which possesses no ^{14}N ligands and thus contributes only to the exponential decay of the modulation pattern and one which is specifically bound to Mnx by just one ^{14}N ligand as described above.

The ESEEM spectrum of RedMnx with 0.8 equiv of Mn(II) is well-simulated assuming a single hyperfine-coupled ^{14}N atom (based on above analysis) to the metal center (blue traces in Figure 8). The ^{14}N magnetic parameters determined from the fit are as follows: A_{iso} = +2.38 ± 0.01 MHz and A_{aniso} = [0.01, 0.20, − 0.21] MHz with nuclear quadrupole parameters e^2Qq/h = 2.35 ± 0.01 MHz and η = 0.22 ± 0.01. Euler angle for quadrupole tensor relative to hyperfine tensor is α = 0 ± 5°, β = 90 ± 5°, γ = 0 ± 5°. An additional damping function (e$^{-\Gamma t}$, $\Gamma \approx$ 0.11 μs^{-1}) was applied to the simulation to model the loss of nuclear coherence due to relaxation. Both hyperfine and nuclear quadrupole parameters are in the range of reported values for

other ^{14}N-coordinated Mn(II) systems (Table 1).[67,68,87−89] The magnitude of the hyperfine interaction measured for the Mnx-bound Mn(II) center (class (ii) is similar to the value for analogous systems with a histidine imidazole serving as a ligand to manganese (cf. Table 1), indicating the ^{14}N-containing ligand could be a imidazole side chain of an active site histidine.

The number of water ligands to this Mnx-bound Mn(II) center was determined using three-pulse ESEEM spectroscopy performed at 327.3 and 363.0 mT as described in the Experimental Procedures section. The ratioed D_2O/H_2O spectrum that contains only modulation from exchangeable deuterons that are hyperfine-coupled to spin centers resonant at $g \approx 2$ is presented in Figure S1A). In this sample, those spin centers include the both the class i and class ii mononuclear Mn(II) species described above. While the sextet observed ca. 330 mT in the X-band CW EPR spectrum arises solely from the aqueous Mn(II) in the sample "RedMnx + 0.8Mn(II)", the echo-detected EPR spectrum possess significant intensity from both types of manganese sites. This is due to the larger ZFS for the class ii site broadening the central field transitions ($\Delta m_S = \pm 1$), allowing them to go undetected in the field-modulated CW experiment (see preliminary simulation in Figure S3).

In the ratioed D_2O/H_2O ESEEM spectrum, we have accounted for the amount of modulation from class i, aqueous Mn(II) in the following way: Using the [Mn(II)] vs EPR signal intensity standard curve described in the Experimental Procedures section, we found that 20% of the total Mn in the sample was of the class i, aqueous Mn(II) type. Preliminary simulations of the CW EPR spectrum achieved using two components (aqueous Mn(II) and bound Mn(II) with ratio of 0.2:0.8) are provided in Figure S4B. We then subtracted a 20% of the residual deuterium modulation for aqueous Mn(II) from that for the "RedMnx + 0.8Mn(II)" sample yielding the red traces in Figure 9. This trace is compared to hypothetical modulation patterns for 1 through 6 water ligands obtained by taking the $N/6$ ($N = 1−6$) root of the D_2O/H_2O ratioed ESEEM spectrum of $[Mn(D_2O)_6]^{2+}$ (black traces in Figure 9). The residual deuterium modulation depth evident in the ratioed spectrum of Mnx-bound Mn(II) corresponds most closely to that for two water ligands ($\approx$1.6 at 327.3 mT and $\approx$1.9 at 363.0 mT).

4. DISCUSSION

The *Bacillus* exosporium multicopper oxidase (MCO) Mnx protein complex plays a central role in manganese biomineralization by catalyzing Mn(II) oxidation to form solid Mn(IV)O$_x$.[11,14,57] While several MCOs that possess metallo-oxidase activity have been characterized previously, all of these systems perform merely one-electron chemistry. Thus, the two-electron oxidation of Mn(II) to Mn(IV) catalyzed by Mnx is mechanistically intriguing.

This process begins with Mn(II) binding to the Mnx complex, presumably in the vicinity of the T1 copper site, in analogous fashion to Fe(II) binding to ceruloplasm (hCp).[15] Results from previous studies of MCOs showed that the reduction potential of the T1 copper site can vary widely from $400 < E_h < 1000$ mV vs NHE and that this variation is usually influenced by the nature of the T1 Cu axial ligand.[13,90,91] While we do not yet know the redox potential of the T1 Cu site in Mnx, if it were as high as +1000 mV, the largest known value for a multicopper oxidase, this would still be insufficient electromotive force to oxidize an aqueous Mn(II) ion to the 3+ oxidation state if the standard-state potentials are used as a

guide ($E° = +1.5$ V vs NHE). These values, of course, correspond to conditions much different than those in effect in the MCO. Alternatively, Mnx could also avoid the reactive and potentially deleterious Mn(III) ion and proceed directly to MnO$_2$(s) from Mn(II) ($E° = +1.23$ V vs NHE), however, this reaction also requires a stronger oxidizing potential from the T1 copper than is likely available. Therefore, the binding site of the substrate must aid in the tuning the redox potential of the Mn(II) ion into an accessible range much as the trigonal bipyramidal active site of Mn-superoxide dismutase does.[52,56,92]

Our EPR spectroscopic studies of fully reduced Mnx treated anaerobically with Mn(II) reveal at least two classes of mononuclear Mn(II)-containing species. One is simply the hexa-aquo Mn(II) substrate that gives rise to the sextet centered at $g = 2$. The other mononuclear Mn(II) species is identified by the appearance of a sextet of transitions at "half-field" ($g \approx 4.0$) that are split by 9.0 mT. Such features are typically diagnostic of a Mn(II) center experiencing modest ZFS interactions ($D < 0.1$ cm^{-1}),[26,27] indicating that the substrate is bound by the Mnx complex with five or six ligands (more likely six). Our ESEEM spectroscopic investigations help to more fully characterize the coordination environment of this bound Mn(II) center. We detect modulations from a single nitrogenous ligand (Figure 6). Based on a comparison between the ^{14}N magnetic parameters for the Mnx-bound Mn(II) derived from simulation of the ESEEM spectra (Figure 8) and those from other studies of Mn(II)−^{14}N-containing spin systems (cf. values in Table 1), we assign this nitrogen as coming from the imidazole side chain of an active site histidine.

Based on our analysis of the ratioed D_2O/H_2O ESEEM data of Mnx-bound Mn(II) (Figure 9), we hypothesize that there are two coordinated water molecules in addition to the histidine ligand. This coordination environment is strikingly similar to that reported for the Mn(II) center in ConA; the X-ray crystal structure and EPR data show that there are one histidine and two water ligands as well as three O donors from proteinacious carboxylate side chains.[93,94] Similarly the MCO hCp binds its substrate Fe(II) with one histidine and three carboxylate ligands.[15] These parallels lead us to propose the Mnx binding environment for the mononuclear Mn(II) center that is depicted in Figure 10. This manganese binding environment is retained for mutant H340A, which gives rise to an almost identical ESEEM spectrum as WT Mnx (Figure S7).
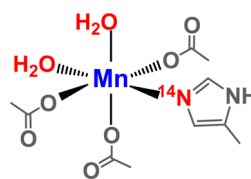

Figure 10. Proposed binding environment of the class ii Mn(II) center bound to the Mnx protein complex. Red colored atoms represent those that were detected from ESEEM measurements. Gray colored atoms are assumed by analogy to hCp and ConA.

A third Mn(II) signal was observed in the EPR spectra of reduced Mnx + Mn(II) that consisted of at least five but perhaps 11 peaks split by a ^{55}Mn hyperfine interaction of approximately 4.5 mT (inset Figure 3). This magnitude of the hyperfine splitting of this feature is very diagnostic of a weakly exchange-coupled Mn(II,II) dimer. This signal is also apparent
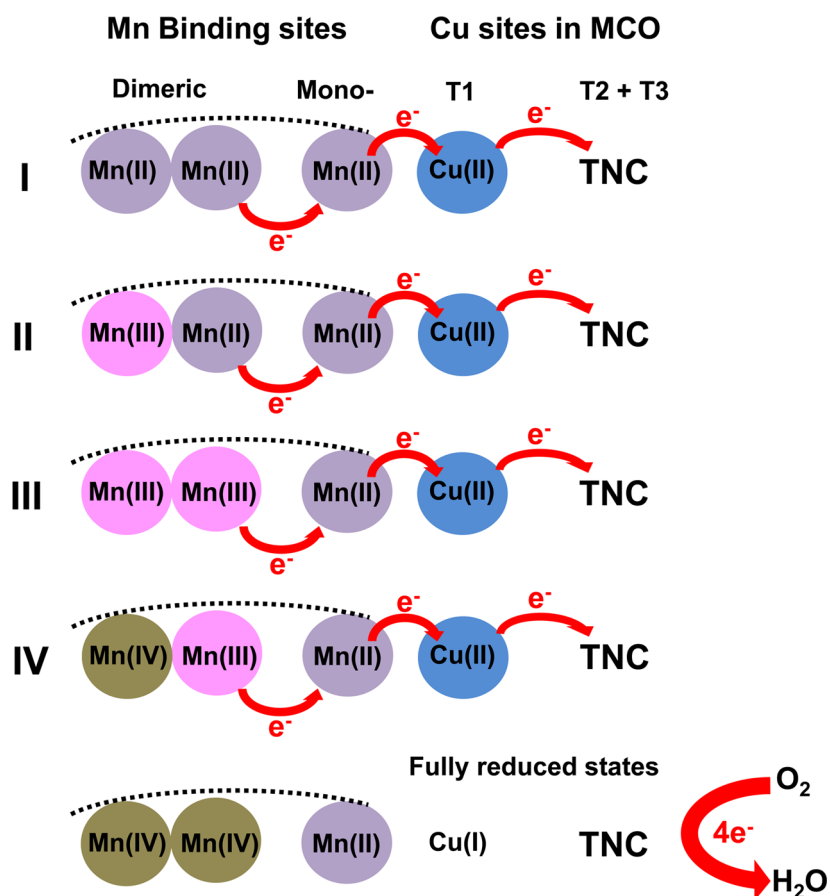
Figure 11. Proposed mechanism for Mn(II) binding and oxidation by the MCO in the Mnx protein complex aerobically.

in spectra of oxidized Mnx mixed with Mn(II) and then rapidly frozen (Figure 1) but requires some time to develop (>10 s). The Mn(II,II) dimer then appears to be oxidized as the signal disappears after 70 s of reaction with O_2. While no mixed-valence dimers were observed, if Mn(III,III)[59] or Mn(IV,IV)[95] dimers were generated, their corresponding EPR spectra are notoriously broad and ill-resolved; thus, it is not surprising that they are non-obvious if present.

The X-band CW EPR spectra show that the aqueous Mn(II) concentration decreases with reaction time via pseudo-first-order kinetics and possibly by two distinct pathways, having rate coefficients of: $k_{1obv} = 0.205 \pm 0.001$ s^{-1} and $k_{2obv} = 0.019 \pm 0.001$ s^{-1}. Previous investigations using either the exosporium from *Bacillus* sp. SG-1 spores[11,57] or purified Mnx protein complex[14] indicate that Mn(III) is generated transiently as the complex Mn(III)pyrophosphate (PP) was observed when enzymatic manganese oxidation was performed in the presence of this strong Mn(III) chelator. These results suggest that Mn(II) oxidation involves two discrete one-electron oxidation steps to generate the Mn(IV) oxide. However, it should be noted that the presence of PP retards Mn(IV) oxide formation by a factor of >100.[11]

Under all of the conditions we employed (notably, always in the absence of PP), we never detected any higher oxidation-state manganese complexes. These included mononuclear Mn(III) or Mn(IV) species which should give rise to diagnostic features in parallel- and perpendicular-polarized EPR spectra, respectively. We also saw no evidence for the generation of antiferromagnetically coupled mixed-valence manganese dimers—either a Mn(II,III) dimer[58] or a Mn(III,IV)

dimer[44,59]—that would yield spin system with an $S = 1/2$ ground electron spin state and give rise to ^{55}Mn hyperfine-split resonances centered at $g = 2$. However, our spectroscopic observation of a Mn(II,II) dimer that disappears in the presence of excess O_2 suggests that higher oxidation-state manganese dimeric species are possible.

Furthermore, it is reasonable that no mononuclear Mn(III) or Mn(IV) species ever accumulate as both are potent oxidants which need to be stabilized by strong donor ligands.[36−40,96,97] Instead, polynuclear Mn(III) or Mn(IV) complexes could be stabilized by oxido-bridging similar to what is prevalent in proteins, such as photosystem II[98−100] and manganese catalases.[101,102] Therefore, we tentatively expect oxidized manganese species in the Mnx protein to oligomerize quickly, giving rise to homovalent dimers (or higher order multimers).

Given all these data, we propose a possible mechanism for the oxidation of Mn(II) by the Mnx enzyme similar to (or consistent with) that proposed by Soldatova et al. (Figure 11).[11] The mononuclear Mnx-bound Mn(II) is assumed to be adjacent to the T1 copper site (again, by analogy to several other MCOs). When the MCO is fully oxidized, this Mn(II) site gets rapidly oxidized to the 3+ state. This resultant Mn(III) could then abstract electrons from the nearby binuclear Mn(II) complex, driven by the formation of hydroxido or oxido-bridges from coordinated water molecules.[11] In this way, the mononuclear Mn(II) center serves as an electron shuttle from the binuclear site to the coppers of the MCO. Upon completion of four electron transfers, the nascent [Mn-(IV)$_2$O$_2$]$^{2+}$ unit will be formed. However, it is difficult to imagine that this happens as described, as solid MnO$_2$ would

soon clog the substrate channel into the MCO active site. Therefore, it is interesting to think about extending this model to include multiple Mn(II) binding sites in Mnx that represent a so-called manganese wire. At the termination of this wire, in the extracellular space, the resultant Mn_xO_{2y} synthon can migrate and nucleate at a nearby site to begin synthesis of the extended solid MnO_2. This mechanism is rather similar to that employed by the iron storage protein ferritin in which Fe(II) is oxidized in binuclear sites to form a dinuclear Fe(III) species which is then transferred along a protein channel to the nucleation sites.[103−105]

ASSOCIATED CONTENT

ⓢ Supporting Information

The Supporting Information is available free of charge on the ACS Publications website at DOI: 10.1021/jacs.5b04331.

> Standard spectra for water-counting via three-pulse ESEEM; electronic absorption spectrum and CW EPR data and simulations of H340A Mnx; echo-detected X-band field swept EPR spectrum of RedMnx + 0.8 Mn(II); and Fourier transform of three-pulse ESEEM data from Figure 7B (PDF)

AUTHOR INFORMATION

Corresponding Author

*rdbritt@ucdavis.edu

Notes

The authors declare no competing financial interest.

ACKNOWLEDGMENTS

REFERENCES

(1) Tebo, B. M.; Bargar, J. R.; Clement, B. G.; Dick, G. J.; Murray, K. J.; Parker, D.; Verity, R.; Webb, S. M. *Annu. Rev. Earth Planet. Sci.* **2004**, *32*, 287.

(2) Spiro, T. G.; Bargar, J. R.; Sposito, G.; Tebo, B. M. *Acc. Chem. Res.* **2010**, *43*, 2.

(3) Morgan, J. J. *Geochim. Cosmochim. Acta* **2005**, *69*, 35.

(4) Nealson, K. H.; Tebo, B. M. *Origins Life* **1980**, *10*, 117.

(5) Geszvain, K.; McCarthy, J. K.; Tebo, B. M. *Appl. Environ. Microbiol.* **2013**, *79*, 357.

(6) Ridge, J. P.; Lin, M.; Larsen, E. I.; Fegan, M.; McEwan, A. G.; Sly, L. I. *Environ. Microbiol.* **2007**, *9*, 944.

(7) Corstjens, P. L. A. M.; de Vrind, J. P. M.; Goosen, T.; Jong, E. W. d. V. d. *Geomicrobiol. J.* **1997**, *14*, 91.

(8) Francis, C. A.; Tebo, B. M. *Appl. Environ. Microbiol.* **2002**, *68*, 874.

(9) Dick, G. J.; Torpey, J. W.; Beveridge, T. J.; Tebo, B. M. *Appl. Environ. Microbiol.* **2008**, *74*, 1527.

(10) Waasbergen, L. G.; Hildebrand, M.; Tebo, B. M. *J. Bacteriol.* **1996**, *178*, 3517.

(11) Soldatova, A. V.; Butterfield, C.; Oyerinde, O. F.; Tebo, B. M.; Spiro, T. G. *J. Biol. Inorg. Chem.* **2012**, *17*, 1151.

(12) Solomon, E. I.; Sundaram, U. M.; Machonkin, T. *Chem. Rev.* **1996**, *96*, 2563.

(13) Solomon, E. I.; Szilagyi, R. K.; George, S. D.; Basumallick, L. *Chem. Rev.* **2004**, *104*, 419.

(14) Butterfield, C. N.; Soldatova, A. V.; Lee, S. W.; Spiro, T. G.; Tebo, B. M. *Proc. Natl. Acad. Sci. U. S. A.* **2013**, *110*, 11731.

(15) Lindley, P. F.; Card, G.; Zaitseva, I.; Zaitsev, V.; Reinhammar, B.; Selin-Lindgren, E.; Yoshida, K. *J. Biol. Inorg. Chem.* **1997**, *2*, 454.

(16) Machonkin, T. E.; Solomon, E. I. *J. Am. Chem. Soc.* **2000**, *122*, 12547.

(17) Heppner, D. E.; Kjaergaard, C. H.; Solomon, E. I. *J. Am. Chem. Soc.* **2013**, *135*, 12212.

(18) Lee, S. K.; George, S. D.; Antholine, W. E.; Hedman, B.; Hodgson, K. O.; Solomon, E. I. *J. Am. Chem. Soc.* **2002**, *124*, 6180.

(19) Solomon, E. I.; Augustine, A. J.; Yoon, J. *Dalton Trans.* **2008**, *30*, 3921.

(20) Schmidt, T. G.; Skerra, A. *Nat. Protoc.* **2007**, *2*, 1528.

(21) Butterfield, C., Ph.D., Oregon Health & Science University, Portland, OR, 2014.

(22) Durão, P.; Chen, Z.; Fernandes, A. T.; Hildebrandt, P.; Murgida, D. H.; Todorovic, S.; Pereira, M. M.; Melo, E. P.; Martins, L. O. *J. Biol. Inorg. Chem.* **2008**, *13*, 183.

(23) Vallejo, A. N.; Pogulis, R. J.; Pease, L. R. *CSH Protoc.* **2008** 10.1101/pdb.prot4861.

(24) Stoll, S.; Schweiger, A. *J. Magn. Reson.* **2006**, *178*, 42.

(25) Stoll, S.; Britt, R. D. *Phys. Chem. Chem. Phys.* **2009**, *11*, 6614.

(26) Reed, G. H.; Markham, G. D. *Bio. Magn. Reson.* **1984**, *6*, 73.

(27) Stich, T. A.; Lahiri, S.; Yeagle, G.; Dicus, M.; Brynda, M.; Gunn, A.; Aznar, C.; DeRose, V. J.; Britt, R. D. *Appl. Magn. Reson.* **2007**, *31*, 321.

(28) Hoogstraten, C. G.; Britt, R. D. *RNA* **2002**, *8*, 252.

(29) Mims, W. B.; Peisach, J. *Biol. Magn. Reson.* **1981**, *3*, 213.

(30) Wijma, H. J.; Boulanger, M. J.; Molon, A.; Fittipaldi, M.; Huber, M.; Murphy, M. E. P.; Verbeet, M. P.; Canters, G. W. *Biochemistry* **2003**, *42*, 4075.

(31) Prudencio, M.; Sawers, G.; Fairhurst, S. A.; Yousafzai, F. K.; Eady, R. R. *Biochemistry* **2002**, *41*, 3430.

(32) Hayden, J. A.; Farquhar, E. R.; Que, L.; Lipscomb, J. D.; Hendrich, M. P. *J. Biol. Inorg. Chem.* **2013**, *18*, 717.

(33) Pierce, B. S.; Elgren, T. E.; Hendrich, M. P. *J. Am. Chem. Soc.* **2003**, *125*, 8748.

(34) Machonkin, E. T.; Quintanar, L.; Palmer, A. E.; Hassett, R.; Severance, S.; Kosman, D. J.; Solomon, E. I. *J. Am. Chem. Soc.* **2001**, *123*, 5507.

(35) Quintanar, L.; Gebhard, M.; Wang, T. P.; Kosman, D. J.; Solomon, E. I. *J. Am. Chem. Soc.* **2004**, *126*, 6579.

(36) Rajendiran, T. M.; Kampf, J. W.; Pecoraro, V. L. *Inorg. Chim. Acta* **2002**, *339*, 497.

(37) Weyhermuller, T.; Paine, T. K.; Bothe, E.; Bill, E.; Chaudhuri, P. *Inorg. Chim. Acta* **2002**, *337*, 344.

(38) Paine, T. K.; Weyhermüller, T.; Bothe, E.; Wieghardt, K.; Chaudhuri, P. *Dalton Trans.* **2003**, 3136.

(39) Parsell, T. H.; Behan, R. K.; Green, M. T.; Hendrich, M. P.; Borovik, A. S. *J. Am. Chem. Soc.* **2006**, *128*, 8728.

(40) Gupta, R.; Taguchi, T.; Borovik, A. S.; Hendrich, M. P. *Inorg. Chem.* **2013**, *52*, 12568.

(41) Mathur, P.; Crowder, M.; Dismukes, G. C. *J. Am. Chem. Soc.* **1987**, *109*, 5227.

(42) Preliminary spectral simulations in support of this assignment are provided in Figure S4. However, given that the only feature we observe experimentally is multiplet at 136.0 mT, we caution the reader from using the given spin Hamiltonian parameters in any meaningful way. They are presented here merely to show that reasonable values for these parameters can give rise to the observed spectral feature.

(43) Similar features have been observed for the Mn(II,II) form of ribonucleotide reductase from *E. coli*.

(44) Cotruvo, J. A.; Stich, T. A.; Britt, R. D.; Stubbe, J. *J. Am. Chem. Soc.* **2013**, *135*, 4027.

(45) Hayden, J. A.; Hendrich, M. P. *J. Biol. Inorg. Chem.* **2010**, *15*, 729.

(46) Reed, G. H.; Ray, W., Jr. *Biochemistry* **1971**, *10*, 3190.

(47) Haffner, P. H.; Goodsaid-Zalduondo, F.; Coleman, J. E. *J. Biol. Chem.* **1974**, *249*, 6693.

(48) Chang, C. H.; Svedruzic, D.; Ozarowski, A.; Walker, L.; Yeagle, G.; Britt, R. D.; Angerhofer, A.; Richards, N. G. *J. Biol. Chem.* **2004**, *279*, 52840.

(49) Reed, G. H.; Morgan, S. D. *Biochemistry* **1974**, *13*, 3537.

(50) Whiting, A. K.; Boldt, Y. R.; Hendrich, M. P.; Wackett, L. P.; Que, L. *Biochemistry* **1996**, *35*, 160.

(51) Burrell, M. R.; Just, V. J.; Bowater, L.; Fairhurst, S. A.; Requena, L.; Lawson, D. M.; Bornemann, S. *Biochemistry* **2007**, *46*, 12327.

(52) Sheng, Y.; Stich, T. A.; Barnese, K.; Gralla, E. B.; Cascio, D.; Britt, R. D.; Cabelli, D. E.; Valentine, J. S. *J. Am. Chem. Soc.* **2011**, *133*, 20878.

(53) Campbell, K. A.; Force, D. A.; Nixon, P. J.; Dole, F.; Diner, B. A.; Britt, R. D. *J. Am. Chem. Soc.* **2000**, *122*, 3754.

(54) Campbell, K. A.; Yikilmaz, E.; Grant, C. V.; Gregory, W.; Miller, A.; Britt, R. D. *J. Am. Chem. Soc.* **1999**, *121*, 4714.

(55) Davies, G. *Coord. Chem. Rev.* **1969**, *4*, 199.

(56) Whittaker, J. W.; Whittaker, M. M. *J. Am. Chem. Soc.* **1991**, *113*, 5528.

(57) Webb, S. M.; Dick, G. J.; Bargar, J. R.; Tebo, B. M. *Proc. Natl. Acad. Sci. U. S. A.* **2005**, *102*, 5558.

(58) Teutloff, C.; Schafer, K. O.; Sinnecker, S.; Barynin, V.; Bittl, R.; Wieghardt, K.; Lendzian, F.; Lubitz, W. *Magn. Reson. Chem.* **2005**, *43*, S51.

(59) Retegan, M.; Collomb, M. N.; Neese, F.; Duboc, C. *Phys. Chem. Chem. Phys.* **2013**, *15*, 223.

(60) Baral, S.; Lume-Pereira, C.; Janata, E.; Henglein, A. *J. Phys. Chem.* **1986**, *90*, 6025.

(61) Rogers, P. A.; Ding, H. *J. Biol. Chem.* **2001**, *276*, 30980.

(62) Epel, B.; Schäfer, K. O.; Quentmeier, A.; Friedrich, C.; Lubitz, W. *J. Biol. Inorg. Chem.* **2005**, *10*, 636.

(63) Golombek, A. P.; Hendrich, M. P. *J. Magn. Reson.* **2003**, *165*, 33.

(64) Khangulov, S. V.; Barynin, V. V.; Voevodskaya, N. V.; Grebenko, A. I. *Biochim. Biophys. Acta* **1990**, *1020*, 305.

(65) Mathur, P.; Dismukes, G. C. *J. Am. Chem. Soc.* **1983**, *105*, 7093.

(66) Golynskiy, M. V.; Gunderson, W. A.; Hendrich, M. P.; Cohen, S. M. *Biochemistry* **2006**, *45*, 15359.

(67) Morrissey, S. R.; Horton, T. E.; Grant, C. V.; Hoogstraten, C. G.; Britt, R. D.; DeRose, V. J. *J. Am. Chem. Soc.* **1999**, *121*, 9215.

(68) Hoogstraten, C. G.; Grant, C. V.; Horton, T. E.; DeRose, V. J.; Britt, R. D. *J. Am. Chem. Soc.* **2002**, *124*, 834.

(69) Espe, M. P.; Hosler, J. P.; Ferguson-Miller, S.; Babcock, G. T.; McCracken, J. *Biochemistry* **1995**, *34*, 7593.

(70) McCracken, J.; Peisach, J.; Bhattacharyya, L.; Brewer, F. *Biochemistry* **1991**, *30*, 4486.

(71) Peters, T.; Blumenstock, F. A. *J. Biol. Chem.* **1967**, *242*, 1574.

(72) Hayden, J. A.; Brophy, M. B.; Cunden, L. S.; Nolan, E. M. *J. Am. Chem. Soc.* **2013**, *135*, 775.

(73) Damo, S. M.; Kehl-Fie, T. E.; Sugitani, N.; Holt, M. E.; Rathi, S.; Murphy, W. J.; Zhang, Y.; Betz, C.; Hench, L.; Fritz, G.; Skaar, E. P.; Chazin, W. J. *Proc. Natl. Acad. Sci. U. S. A.* **2013**, *110*, 3841.

(74) Harford, C.; Sarkar, B. *Acc. Chem. Res.* **1997**, *30*, 123.

(75) Flanagan, H. L.; Singel, D. J. *J. Chem. Phys.* **1987**, *87*, 5606.

(76) Kozlowski, H.; Potocki, S.; Remelli, M.; Rowinska-Zyrek, M.; Valensin, D. *Coord. Chem. Rev.* **2013**, *257*, 2625.

(77) Sankararamakrishnan, R.; Verma, S.; Kumar, S. *Proteins: Struct., Funct., Genet.* **2005**, *58*, 211.

(78) Rozga, M.; Sokolowska, M.; Protas, A. M.; Bal, W. *J. Biol. Inorg. Chem.* **2007**, *12*, 913.

(79) Masuoka, J.; Hegenauer, J.; Dyke, B. R.; Saltman, P. *J. Biol. Chem.* **1993**, *268*, 21533.

(80) Mildvan, A. S.; Cohn, M. *Biochemistry* **1963**, *2*, 910.

(81) Liang, H.; Tu, C.; Zhang, H.; Shen, X.; Zhou, Y.; Shen, P. *Chin. J. Chem.* **2000**, *18*, 35.

(82) The data for CP-bound Mn(II) are reproduced from a recently published EPR study.

(83) Gagnon, D. M.; Brophy, M. B.; Bowman, S. E. J.; Stich, T. A.; Drennan, C. L.; Britt, R. D.; Nolan, E. M. *J. Am. Chem. Soc.* **2015**, *137*, 3004.

(84) Mims, W. B. *Phys. Rev. B* **1972**, *5*, 2409.

(85) Schweiger, A.; Jeschke, G. *Principles of Pulse Electron Paramagnetic Resonance*; Oxford University Press: New York, 2001.

(86) In particular, we are focusing on the first observed beat in the modulation pattern as the different nuclear relaxation behavior for each Mn(II)-containing protein should have negligible effects on the depth of this first modulation.

(87) Ashby, C. I. H.; Cheng, C. P.; Brown, T. L. *J. Am. Chem. Soc.* **1978**, *100*, 6057.

(88) Astashkin, A. V.; Nesmelov, Y. E. *J. Phys. Chem. B* **2012**, *116*, 13655.

(89) Garcia-Rubio, I.; Angerhofer, A.; Schweiger, A. *J. Magn. Reson.* **2007**, *184*, 130.

(90) Quintanar, L.; Stoj, C.; Taylor, A. M.; Hart, P. J.; Kosman, D. J.; Solomon, E. I. *Acc. Chem. Res.* **2007**, *40*, 445.

(91) Xu, F.; Berka, R. M.; Wahleithner, J. A.; Nelson, B. A.; Shuster, J. R.; Brown, S. H.; Palmer, A. E.; Solomon, E. I. *Biochim. Biophys. Acta* **1998**, *334*, 63.

(92) Miller, A. F. *FEBS Lett.* **2012**, *586*, 585.

(93) Sanz-Aparicio, J.; Hermoso, J.; Grangeiro, T. B.; Calvete, J. J.; Cavada, B. S. *FEBS Lett.* **1997**, *405*, 114.

(94) Rozwarski, D. A.; Swami, B. M.; Brewer, C. F.; Sacchettini, J. C. *J. Biol. Chem.* **1998**, *273*, 32818.

(95) Caudle, M. T.; Kampf, J. W.; Kirk, M. L.; Rasmussen, P. G.; Pecoraro, V. L. *J. Am. Chem. Soc.* **1997**, *119*, 9297.

(96) Weiss, R.; Gold, A.; Trautwein, A. X.; Terner, J. In *The porphyrin handbook*; Kadish, K. M., Smith, K. M., Guilard, R., Ed.; Academic: Boston, 2002.

(97) Groves, J. T.; Stern, M. K. *J. Am. Chem. Soc.* **1988**, *110*, 8628.

(98) Ferreira, K. N.; Iverson, T. M.; Maghlaoui, K.; Barber, J.; Iwata, S. *Science* **2004**, *303*, 1831.

(99) Loll, B.; Kern, J.; Saenger, W.; Zouni, A.; Biesiadka, J. *Nature* **2005**, *438*, 1040.

(100) Yeagle, G. J.; Gilchrist, M. L.; McCarrick, R. M.; Britt, R. D. *Inorg. Chem.* **2008**, *47*, 1803.

(101) Barynin, V. V.; Whittaker, M. M.; Antonyuk, S. V.; Lamzin, V. S.; Harrison, P. M.; Artymiuk, P. J.; Whittaker, J. W. *Structure* **2001**, *9*, 725.

(102) Stich, T. A.; Whittaker, J. W.; Britt, R. D. *J. Phys. Chem. B* **2010**, *114*, 14178.

(103) Liu, X.; Theil, E. C. *Acc. Chem. Res.* **2005**, *38*, 167.

(104) Ha, Y.; Shi, D.; Small, G. W.; Theil, E. C.; Allewell, N. M. *J. Biol. Inorg. Chem.* **1999**, *4*, 243.

(105) Turano, P.; Lalli, D.; Felli, I. C.; Theil, E. C.; Bertini, I. *Proc. Natl. Acad. Sci. U. S. A.* **2010**, *107*, 545.